FEBS Letters 589 (2015) 1840–1846

FEBS Letters

journal homepage: www.FEBSLetters.org

Functional characterization of Val60, a key residue involved in the membrane-oligomerization of fragaceatoxin C, an actinoporin from *Actinia fragacea*

Koldo Morante [a,b,c], Jose M.M. Caaveiro [c], Ana Rosa Viguera [a], Kouhei Tsumoto [c,d,e], Juan Manuel González-Mañas [b,*]

[a] Biophysics Unit (CSIC, UPV/EHU), University of the Basque Country, P.O. Box 644, 48080 Bilbao, Spain
[b] Department of Biochemistry and Molecular Biology, University of the Basque Country, P.O. Box 644, 48080 Bilbao, Spain
[c] Department of Bioengineering, Graduate School of Engineering, The University of Tokyo, Minato-ku 108-8639, Tokyo, Japan
[d] Medical Proteomics Laboratory, Institute of Medical Science, The University of Tokyo, Minato-ku 108-8639, Tokyo, Japan
[e] Department of Medical Genome Sciences, Graduate School of Frontier Sciences, The University of Tokyo, Minato-ku 108-8639, Tokyo, Japan

ARTICLE INFO

Article history:
Received 21 February 2015
Revised 29 May 2015
Accepted 1 June 2015
Available online 19 June 2015

Edited by Peter Brzezinski

Keywords:
Pore-forming toxins
Protein oligomerization
Lipid–protein interaction
Model membranes

ABSTRACT

Actinoporins are pore-forming toxins produced by different sea anemones that self-assemble within the membranes of their target cells and compromise their function as a permeability barrier. The recently published three-dimensional structures of two oligomeric complexes formed by fragaceatoxin C point to Val60 as a key residue involved in the oligomerization of the functional pore.

To gain insight into the mechanism of toxin oligomerization, different point mutations have been introduced at this position. Functional characterization of the muteins suggests that Val60 represents a hot-spot where the introduction of mutations hinders protein assembly and reduces the overall affinity for membranes.

1. Introduction

The lytic mechanism of a wide variety of pore-forming toxins (PFT) involves an oligomerization step that leads to the assembly of the fully functional pore. Oligomerization can be induced by binding to other molecules [1] or by environmental factors such as fluctuations in pH [2], temperature [3], or hydrophobicity [4]. Actinoporins are a well-known example of membrane-induced oligomerization, since the presence of a lipid bilayer is strictly necessary to trigger the construction of the active pore [5].

In oligomeric PFT, the protomers are held together mainly by electrostatic forces, as in *Vibrio cholerae* cytolysin (VCC) [6] or *Staphylococcus aureus* α- and γ-hemolysins [7,8], although non-polar interactions have also been described for the so-called latch structure described in *S. aureus* hemolysins, where isoleucine and valine residues interact at the protomer–protomer interface [4,7].

Recently, the three-dimensional structures of two oligomeric complexes formed by fragaceatoxin C (FraC), an actinoporin from the sea anemone *Actinia fragacea*, have been reported (PDB codes: 3LIM and 4TSY) [5,9]. In both structures, the interface between adjacent subunits exhibits high shape complementarity and resembles a mortise-and-tenon joint, where Val60 from one protomer protrudes into a cavity within the opposing protomer lined by two (4TSY) or three (3LIM) aromatic residues, namely Phe16, Trp149 and Phe163 (Fig. 1A) [5,9]. Curiously, Val60 is one of the residues with highest buried surface area (95.5 ± 1.2 Å^2) and establishes a number of contacts with the residues lining the aromatic cavity [5]. Moreover, Val60 is a highly conserved residue within actinoporins (Fig. 1B). These features strongly suggest a key role

Abbreviations: PFT, pore-forming toxins; FraC, fragaceatoxin C; RBC, red blood cells; SM, sphingomyelin; PC, chicken egg L-α-phosphatidylcholine; LUV, large unilamellar vesicle; SEC, size-exclusion chromatography; DDM, *n*-dodecyl β-D-maltopyranoside; HC_{50}, protein concentration required for 50% lysis; T_M, denaturation temperature; CD, circular dichroism

Author contributions: K.M., J.M.M.C. and A.R.V. performed experiments; J.M.M.C., J.M.G.M. and K.T. conceived and supervised the study; K.M., J.M.M.C. and J.M.G.M. analyzed data; K.M., J.M.M.C. and J.M.G.M. wrote the manuscript.

* Corresponding author. Fax: +34 94 6013500.
E-mail address: juanmanuel.gonzalez@ehu.es (J.M. González-Mañas).

http://dx.doi.org/10.1016/j.febslet.2015.06.012
0014-5793/

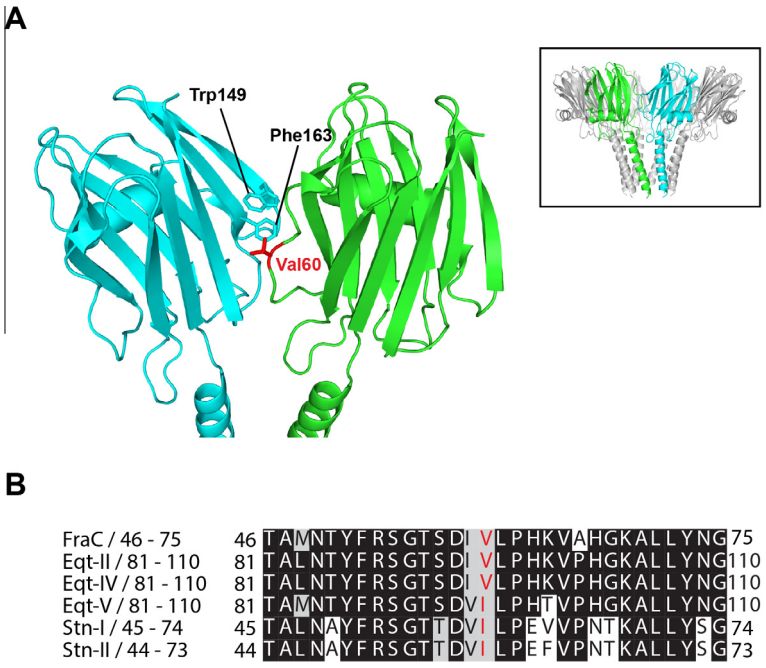

Fig. 1. Protomer–protomer interface in the membrane-inserted oligomeric FraC pore. (A) Val60 (red) from one protomer (green) protrudes into an aromatic pocket in the adjacent subunit (cyan). The aromatic cavity is lined by residues Trp149 and Phe163. The complete octameric pore is shown in the inset (PDB entry 4TSY). (B) Multiple sequence alignment of actinoporins with known crystal structure. The residue at position 60 is depicted in red. The alignment was performed with CLUSTALW2 and shaded with BoxShade.

for Val60 in monomer assembly and it seemed to be the candidate of choice to further examine the oligomerization step that takes place during the mechanism of pore formation by FraC.

For this purpose, we introduced several point mutations at position 60 in order to determine how these changes affected the activity of FraC. Val60 was replaced by arginine (V60R), lysine (V60K), glutamic acid (V60E) or phenylalanine (V60F). Amino acids Arg, Lys, and Glu were expected to introduce polar–apolar repulsions within the adjacent aromatic pocket, whereas Phe was expected to alter the shape complementarity between adjacent protomers.

Functional data based on experiments carried out on red blood cells (RBC) or model membranes confirmed the relevance of Val60 in mediating proteomer–protomer interactions for the correct assembly of FraC subunits, a key step leading to the formation of the functional pore.

2. Materials and methods

2.1. Protein expression and purification

Expression and purification of monomeric FraC was carried out as previously described [10], with minor modifications. Growth and expression were induced by 0.5 mM IPTG for 20 h at 20 °C. The protein was then purified to homogeneity in two chromatographic steps involving a Resource S cationic-exchange column (GE Healthcare, Piscataway, NJ, USA) and a HiLoad 16/60 Superdex 75 prep grade column (GE Healthcare, UK). Site-directed mutagenesis to generate the various muteins was carried out as in [11].

2.2. Hemolytic activity measurements

Defibrinated sheep blood (Pronadisa, Madrid, Spain) was washed in 5 mM sodium phosphate buffer, 150 mM NaCl, pH 8. After incubation of a fixed concentration of RBC (3×10^6 cells/ml) with a variable concentration of protein in a 96-well plate for 90 min at room temperature, the total hemoglobin released from the cells was measured as A_{412}. The percentage of hemolysis was then calculated as:

$$\text{Hemolysis } (\%) = (A_{max} - A_{fin})/(A_{max} - A_{min}) \times 100$$

where A_{fin} corresponds to the final absorbance measured for each well. A_{max} and A_{min} represent the A_{412} values for 100% and 0% hemolysis achieved with distilled water and buffer, respectively.

2.3. Liposome preparation

Brain porcine sphingomyelin (SM) and chicken egg L-α-phosphatidylcholine (PC) (Avanti Polar Lipids, AL, USA) were dissolved in chloroform:methanol (2:1, v/v) and evaporated thoroughly. The dry lipid film was resuspended by vortexing in 50 mM NaCl, 10 mM HEPES-NaOH, pH 7.5 containing 25 mM 8-aminonaphthalene-1,3,6-trisulfonic acid (the fluorophore) and 90 mM *p*-xylene-bis-pyridinium bromide (the quencher) (Molecular Probes, OR, USA) to yield multilamellar vesicles that subsequently were subjected to 10 cycles of freeze–thaw as previously described [10]. Large unilamellar vesicles (LUV) were prepared by extrusion through polycarbonate filters with a pore diameter of 0.1 μm (Nucleopore, Pleasanton, CA, USA) [12]. Non-encapsulated fluorescent probes were separated from the vesicle suspension through a Sephadex G-25 column (Amersham Biosciences, GE Healthcare, UK) eluted with isosmotic 10 mM HEPES-NaOH, 200 mM NaCl, pH 7.5. Phospholipid concentration was measured according to Bartlett [13].

2.4. Leakage of encapsulated solutes

The leakage of encapsulated solutes was assayed as described by Ellens [14]. Briefly, the fluorescence of LUV suspensions (0.1 mM) treated with FraC (0.67 μM) was followed with excitation and emission wavelengths set at 355 nm and 515 nm, respectively. An absorption filter of 475 nm was placed between the sample and

the emission monochromator. Complete release of the fluorescent probe was achieved by the addition of Triton X-100 (final concentration 0.1% w/v). The percentage of leakage was calculated as follows:

$$\%\ \text{Leakage} = (F_f - F_0/F_{100} - F_0) \times 100$$

where F_f is the fluorescence measured after addition of the toxin, F_0 is the initial fluorescence of the liposome suspension and F_{100} is the fluorescence after addition of detergent. Measurements were carried out at room temperature with constant stirring in a FluoroMax-3 spectrofluorometer (Horiba Jobin Yvon, Kyoto, Japan).

2.5. Purification of oligomeric FraC

Toxins (100 μM) were incubated with LUVs (200:1 lipid:protein molar ratio) in 50 mM Tris–HCl, 200 mM NaCl pH 7.4 buffer (SEC buffer) for 30 min at room temperature. The proteo-liposome complex was solubilized by adding Triton X-100 to the mixture at a final concentration of 1% (v:v). The sample (approximately 500 μl in volume) was then diluted 20-fold in 50 mM Tris–HCl, 0.3 mM DDM pH 7.4 (buffer A) and applied to a Resource S cationic-exchange column. To elute the protein, a linear salt gradient was formed by mixing buffer A with 50 mM Tris–HCl, 1 M NaCl, 0.3 mM DDM pH 7.4 (buffer B). Fractions were then analyzed by size-exclusion chromatography in a Superdex 200 10/300 GL column equilibrated with SEC buffer supplemented with 0.3 mM DDM. The presence of protein in the elution peaks was verified by SDS–PAGE.

2.6. Surface pressure measurements

Surface pressure measurements were carried out by the Wilhelmy plate method [15] using a Micro-Trough-S system from Kibron (Helsinki, Finland) at room temperature with constant stirring. In this method, the tip of a titanium probe connected to an electrobalance is submerged in an aqueous solution. At the air–water interface, the surface tension of the water molecules exerts a downward force on the probe which is registered by the electrobalance. The displacement of water molecules from the air–water interface by amphiphilic molecules injected in the aqueous subphase results in changes in the weight of the probe that are monitored and recorded. Surface tension measurements are readily converted to surface pressure values (π) by subtracting the surface tension of the sample from that of the pure solvent, which in the case of water is 72.8 mN/m.

The aqueous subphase consisted of 1 ml of 10 mM HEPES-NaOH, 200 mM NaCl, pH 7.5. A lipid mixture containing the adequate proportions of SM and PC dissolved in chloroform/methanol (2:1, v/v), was gently spread over the air–water interface. The desired initial surface pressure was attained by applying different amounts of lipid. After 10 min (to allow for solvent evaporation) the protein was injected into the subphase at a final concentration of 1 μM and the resulting increment in surface pressure ($\Delta\pi$) recorded. To calculate the surface pressure after maximum insertion, a three-parameter rectangular hyperbola [16] was fitted to the kinetic data:

$$y = y_0 + (a \cdot x/b + x)$$

where y is $\Delta\pi$, y_0 is the initial surface pressure (π_0), a is the maximum surface pressure achieved and b is a constant that represents the time necessary to reach half of the maximum increase. The critical pressure (π_c) was obtained by solving the above equation when $y = 0$.

2.7. Thermal stability by circular dichroism (CD)

Thermal denaturation was monitored using a J-820 spectropolarimeter (Tokyo, Japan) equipped with a Jasco PTC-423L temperature controller in 1 mm quartz cuvettes. Unfolding of the toxins in 20 mM Tris–HCl pH 8 was monitored at 210 nm using a heating rate of 1 °C/min and a 2 nm band-width. Denaturation temperatures (T_M) were calculated by fitting a two-state model equation to the experimental data [17]:

$$\text{Protein unfolding}\ (\%) = [k/(1+k)]100$$

where k is the folding constant and is expressed as:

$$k = exp[(\Delta H/(1.987T)) \cdot ((T/T_M) - 1)]$$

where T_M is the temperature at which the protein is 50% unfolded, ΔH is the change in enthalpy, and T is the temperature.

2.8. Isothermal titration calorimetry (ITC)

The interaction between toxins and liposomes was measured with an ITC200 Micro Calorimeter (GE Healthcare, UK) in SEC buffer at 25 °C. The LUV suspension was injected into a cell containing protein under constant stirring. The heat released after each injection was determined from the raw data by integration of the individual exothermic peaks after subtraction of the baseline. The model used to fit the binding isotherms considered that a molecule of protein binds to n molecules of lipid and is incorporated into the software ORIGIN 7 as described previously [18]. Each titration was repeated at least twice.

3. Results

3.1. Hemolytic activity and protein stability

The hemolytic potency of the muteins was compared with that of wild-type FraC (WT). Fig. 2A shows the percentage of hemoglobin released from RBC treated with the toxins over a broad range of concentrations. The strongest inhibitory effect was observed with V60E. The concentration of V60E that causes 50% hemolysis (HC_{50}) was approximately 30-fold higher than that of WT ($HC_{50}{}^{WT}$ = 2.4 ± 0.3 nM; $HC_{50}{}^{V60E}$ = 67.6 ± 6.9 nM). The hemolytic activity of the other muteins was also reduced, but to a lesser extent ($HC_{50}{}^{V60R}$ = 18.0 ± 4.3 nM; $HC_{50}{}^{V60K}$ = 13.8 ± 0.7 nM; $HC_{50}{}^{V60F}$ = 16.7 ± 4.1 nM), thus confirming the key role played by Val60 in protein–protein interactions during pore formation.

The decreased activity could be due to changes in thermal stability introduced by the various point mutations. To rule out this possibility, we determined the protein denaturation temperature (T_M) of the different toxins by measuring their molar ellipticities in a broad temperature range (25–70 °C) (Fig. 2B). In all cases, the unfolding profiles were very similar (T_M^{WT} = 53.2 °C; T_M^{V60E} = 54.1 °C; T_M^{V60R} = 55.1 °C; T_M^{V60K} = 54.8 °C; T_M^{V60F} = 51.3 °C) (Fig. 2B) and might not explain the poor hemolytic activity of the muteins. This is particularly evident in the case of V60E, whose T_M is very to that of the WT but hardly conserves hemolytic activity.

3.2. Interaction with model membranes

The lytic activity of WT and muteins was measured as the release of fluorescent contents from LUVs made of SM:PC (1:1) (Fig. 3A and Table 1). The results correlate well with those observed in RBCs (Fig. 2A): whereas V60E lacked lytic activity (0% leakage), the activity of the other muteins was approximately one third of that of WT (Table 1).

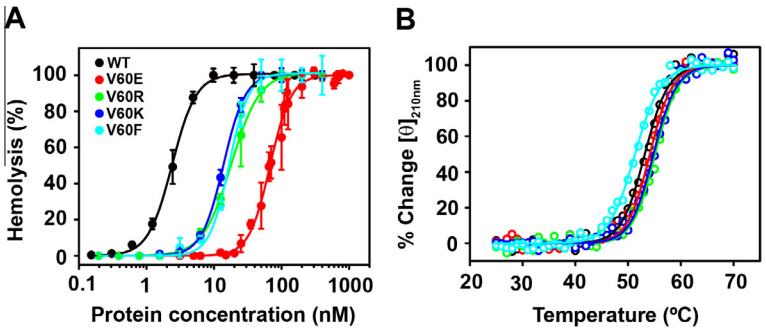

Fig. 2. Biological activity and stability. (A) Percentage of hemolysis as a function of protein concentration. The curves correspond to the best fit to the Hill equation [31]. (B) Thermal denaturation curves of WT and muteins measured as the percentage of change in ellipticity at 210 nm. A two-state model equation was fitted to the data points (see Section 2). The color code for each protein is shown in panel A.

From the percentage leakage *vs.* protein concentration range we estimated the concentration of protein necessary to achieve 50% lysis (C_{50}) (Fig. 3B and Table 1). The C_{50} was highest for V60E (C_{50} = 4.4 ± 0.26 μM) and lowest for WT (C_{50} = 0.3 ± 0.01 μM). The other muteins showed C_{50} intermediate values close to 1 μM but, interestingly, the dependence of their permeabilizing activities on protein concentration was different, as inferred from the slope of the sigmoid curves. This could be related to a decrease in cooperativity that affects in a different way to each mutein and interferes with the oligomerization process.

Next, we carried out size-exclusion chromatographic analysis in order to determine if oligomers were produced by the different muteins. Fig. 3C shows the elution profiles of WT and the least active mutein (V60E). In aqueous solution, the elution volumes of WT and V60E are 27.9 ± 0.1 ml and 27.2 ± 0.1 ml, respectively and these peaks are attributed to the monomeric species. These volumes are higher than the column bed volume corresponding to the column (∼ 20.5 ml). Most likely, this is due to non-specific interactions with the column's matrix [19]. After incubation of the vesicles with either toxin, a new peak appears at 12.2 ± 0.1 ml. This peak contains protein as judged by SDS–PAGE analysis (Fig. 3D) and might correspond to solubilized membrane-bound oligomers. This peak represents 86% of the total protein in the case of WT and 19% of the protein in the case of V60E (Fig. 3C and Table 1). Most of V60E (81%) eluted at 26.22 ± 0.1 ml, which is consistent with a monomeric species with some bound lipid and/or detergent molecules [9].

The other muteins showed similar elution profiles, although the distribution between oligomers and monomers was not as extreme (Supplementary Fig. 1A and Table 1).

The interaction of the toxins with lipid monolayers made of SM:PC (1:1) was measured by monitoring the $\Delta\pi$ induced after injection of the proteins in the aqueous subphase (Fig. 3E). The critical pressure parameter (π_c) indicates the surface pressure of the monolayer above which a protein can no longer insert. In biological membranes, this surface pressure is approximately 30–35 mN/m [20]. Consequently, proteins with π_c below this value would be unable to insert. The π_c value for WT is 36 ± 1.1 mN/m. The critical pressures for the muteins are slightly lower ($\pi_c^{muteins} \approx 30$ mN/m) but still in the range where they can theoretically insert into a biological membrane (Fig. 3E, Table 1) [21].

3.3. Calorimetric studies

Isothermal titration calorimetry (ITC) was used for the thermodynamic characterization of the binding of the toxins to LUVs made of SM:PC (1:1). The binding of WT FraC (Fig. 4A) is enthalpy-driven ($\Delta H°_{WT} = -9.9 \pm 0.5$ kcal mol^{-1}) and shows moderate affinity for lipids (K_D^{WT} = 16 ± 9 μM; $\Delta G° = -6.5 \pm 0.3$ kcal mol^{-1}). The enthalpic component is partially compensated by the entropic component ($-T\Delta S° = 3.3 \pm 0.8$ kcal mol^{-1}), as previously described for sticholysin II and FraC in other lipid mixtures [18,22]. In contrast, binding of V60E to liposomes generated a weak exothermic signal, nor sufficient for a reliable quantification of the thermodynamic parameters (Fig. 4B).

4. Discussion

During evolution proteins have found ways to acquire structural and/or functional advantages by assembling with other proteins (identical or not) into oligomeric complexes [23]. For instance, protein oligomerization provides enzymes with an increased stability or a better regulation of their activity, as highlighted by thermostable or allosteric enzymes [24,25].

In actinoporins, oligomerization is a key step for the assembly of the functional pore. For some decades, important residues involved in the oligomerization of these toxins have remained elusive. Only residue Lys77 in equinatoxin II has been related to this process [26]. This scenario changed completely after the crystal structures of two oligomeric complexes formed by FraC were solved [5,9]. They form a protein ring where the contact surfaces involved in protein–protein interactions are rather small (∼777 Å^2) [9] but exhibit high shape complementarity (0.66) [5], very close to that of antibody-antigen complexes [27]. Curiously, Lys77 does not lie within this region [9]. The position of Val60, however, suggests that this residue is central for the correct assembly of the protomers. Its side chain presents the second highest buried surface area (95.5 ± 1.2 Å^2) because it occupies an aromatic cavity within the adjacent subunit (Trp149 is the residue with highest buried surface area: 115.1 ± 5.7 Å^2). Point mutations introduced at this position are expected to greatly interfere with the assembly of the pore.

Of all the residues introduced at position 60 of FraC, only the glutamic acid showed an almost complete inhibition of lytic activity. This is not due to impaired binding to the membrane, since its insertion into lipid monolayers is identical to that of the other muteins (Fig. 3E). Therefore, the disruption must arise during the oligomerization step. A further look at the structure of the aromatic pocket housing Val60 reveals a glutamic acid residue (Glu173) 2.3 Å away from Val60. The slightly longer side chain of V60E would lie even closer and, most likely, will give rise to an electrostatic repulsion between adjacent protomers. As a consequence, the population of fully-assembled pores would be greatly reduced (Fig. 3C), thus leading to a considerably lower lytic activity in RBC and liposomes (Figs. 2A and 3B).

On the other hand, the positively-charged residues arginine and lysine at position 60 might establish salt bridges with Glu173 that result in a ∼13% reduction in the number of oligomers formed

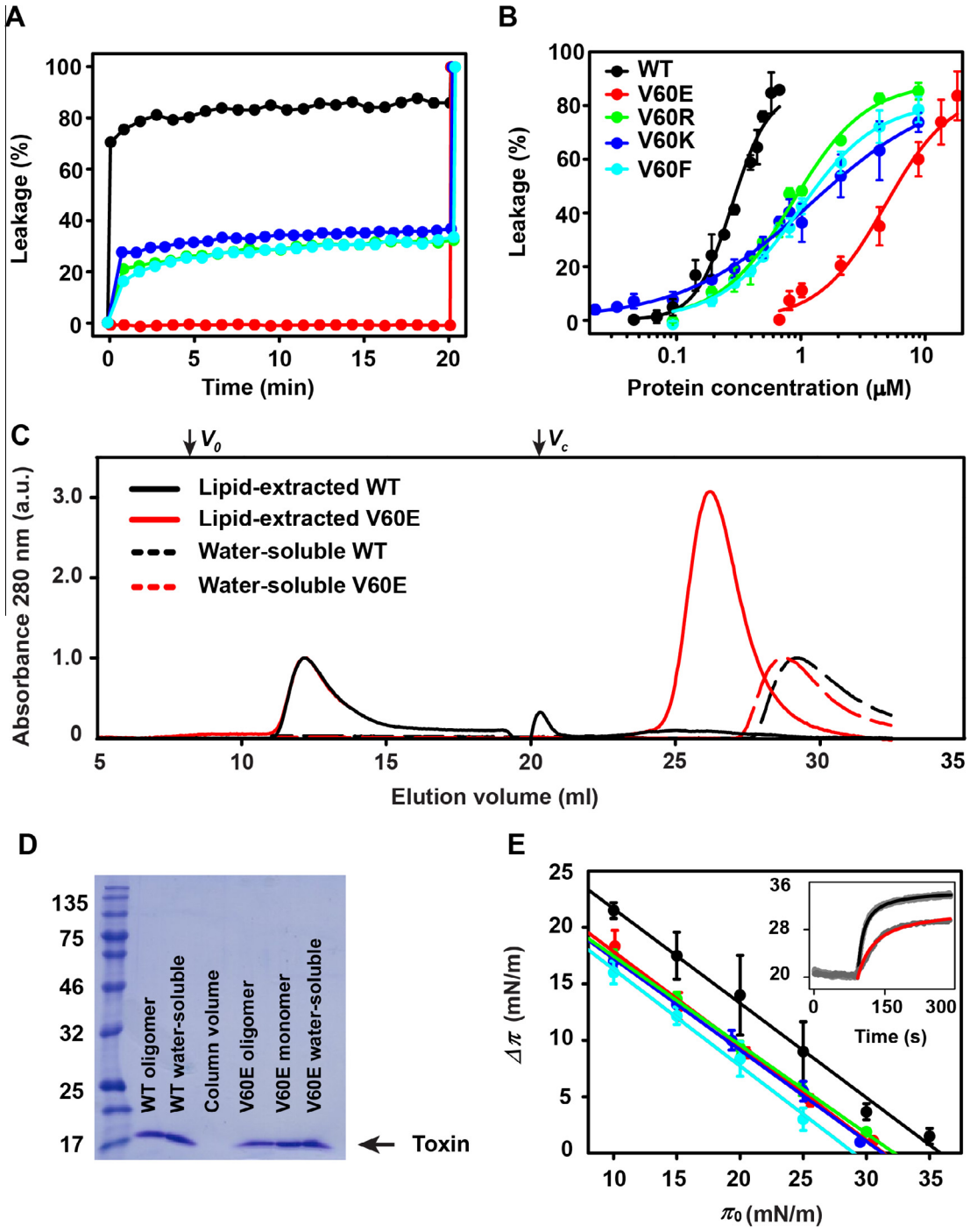

Fig. 3. Activity and interaction of FraC with model membranes of SM:PC (1:1). (A) Leakage kinetics as measured by the release of encapsulated solutes from LUV. Lipid concentration was 100 μM and the lipid:protein molar ratio was 150:1. (B) Dependence of solute release on protein concentration. The final fluorescence was measured 20 min after protein addition (Table 1). The curves correspond to the best fit to the Hill equation [31]. (C) SEC chromatogram of WT (black) and V60E (red) purified after incubation with lipids. The amount of protein injected was 31 μg for WT and 84 μg for V60E. The elution volumes for blue dextran (V_0) and the column bed volume (V_c) are indicated by arrows. The black (WT) and red (V60E) dashed lines correspond to the elution peaks not incubated with liposomes, *i.e.* the water-soluble form. The absorbance fluctuations observed at ~20 ml are related to the changes in conductivity at V_c. (D) SDS–PAGE of the peaks in panel C. The amount protein in each well corresponds to ~2.6 ng of protein. (E) Plot representing $\Delta\pi$ *vs.* π_0 values extracted from monolayer experiments. Fitting a linear equation to the data points gives the value for π_c (intercept at $y = 0$). Inset: surface pressure kinetic measurements of WT (black) and V60E (red) from where the values for $\Delta\pi$ and π_0 were extracted. The color code for each protein is shown in panel B.

(Supplementary Fig. 1A and Table 1) that accounts for the moderate lytic activity exhibited by V60R and V60K (Figs. 2A, 3A and B). Again, this inhibition is not due to lack of binding (Fig. 3E).

In the case of V60F, the introduction of a bulky phenylalanine might add steric clashes to the protomer–protomer interaction that result in a ~24% reduction in the number of oligomers formed (Supplementary Fig. 1A and Table 1) and an intermediate permeabilizing activity (Figs. 2A, 3A and B).

The oligomerization mechanism of FraC (and actinoporins in general) is rather simple when compared to other PFT where large rearrangements take place [4,6,28]. Protomer–protomer interactions in β-PFT and cytolysin A commonly involve large interfaces

Table 1
Parameters extracted from the behavior of the toxins in red blood cells and model membranes of SM:PC (1:1).

Protein	Hemolysis[a]	Activity on LUVs[b]		SEC analysis[c]		Monolayers[d]
	HC_{50} (nM)	Leakage (%)	C_{50} (μM)	Oligomer (%)	Monomers (%)	π_c (mN/m)
WT	2.4 ± 0.3	86 ± 2	0.29 ± 0.01	86	14	36 ± 1.1
V60E	67.6 ± 6.9	0 ± 1	4.42 ± 0.26	19	81	31 ± 0.1
V60R	18.0 ± 4.3	32 ± 3	0.85 ± 0.08	74	26	31 ± 0.6
V60K	13.8 ± 0.7	36 ± 2	1.18 ± 0.36	76	24	32 ± 1.4
V60F	16.7 ± 4.1	32 ± 2	0.94 ± 0.11	65	35	29 ± 2

The values correspond to the means of two or three independent measurements ± their standard deviations.
[a] Refer to Fig. 2A.
[b] Refer to Fig. 3A and B. Leakage values correspond to a protein concentration of 0.67 μM.
[c] Refer to Fig. 3C and Fig. 1 in the supplementary information.
[d] Refer to Fig. 3D.

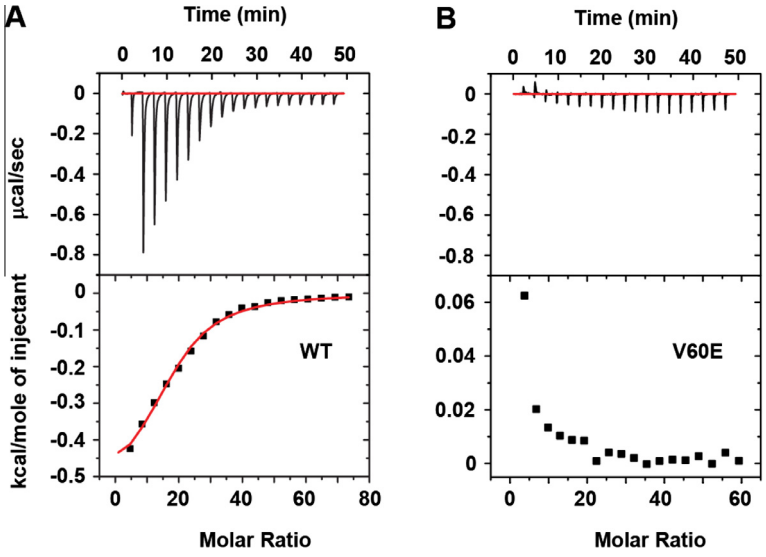

Fig. 4. Isothermal titration calorimetry of the toxin-lipid interaction. Thermal titration of WT (43 μM) (A) and V60E (51 μM) (B) with LUV of SM:PC (1:1). The top panel corresponds to the titration kinetics and the bottom panel to the binding isotherm. The concentration of lipid in the syringe was 16.2 mM in panel A and 15.5 mM in panel B. The molar ratio refers to lipid/protein. For the thermodynamic parameters refer to the text.

comprising ~14% of the buried surface per monomer, where electrostatic interactions predominate [4,7,28]. In contrast, in FraC the contact surfaces involved in protein–protein interactions are rather small (~8% of the buried surface per monomer) [9] and might compromise the stability of the oligomer. To compensate for this apparent lack of stability, actinoporins might have evolved solvent exposed residues like Val60 that create patches with high shape complementarity at the protein–protein interface. These regions represent hot-spots that govern protein assembly [29] and the introduction of mutations at this position not only hinders protein assembly but its overall affinity for membranes as well (Fig. 4).

In summary, oligomerization of proteins might have evolved as an adaptation to associate with hydrophobic media following a favorable energetic pathway. For monomeric proteins, the insertion of β-hairpins or amphipathic α-helices across the membrane would be costly in energetic terms. The development of alternative cooperative strategies [30] would help to promote the formation of stable water-filled pathways across the lipid milieu.

Acknowledgments

This study was supported by the Funding Program for World-Leading Innovative R&D on Science and Technology (FIRST) of the Japan Society for the Promotion of Science and by the Platform for Drug Discovery, Informatics, and Structural Life Science of the Ministry of Education, Culture, Sports, Science and Technology of Japan. Koldo Morante was recipient of a fellowship from the Spanish Ministerio de Ciencia e Innovación.

Appendix A. Supplementary data

Supplementary data associated with this article can be found, in the online version, at http://dx.doi.org/10.1016/j.febslet.2015.06.012.

References

[1] Matthews, J.M. (2012) Protein Dimerization and Oligomerization in Biology, Springer, New York.
[2] Allison, S.L., Schalich, J., Stiasny, K., Mandl, C.W., Kunz, C. and Heinz, F.X. (1995) Oligomeric rearrangement of tick-borne encephalitis virus envelope proteins induced by an acidic pH. J. Virol. 69, 695–700.
[3] Li, K., Jiang, T., Yu, B., Wang, L., Gao, C., Ma, C., Xu, P. and Ma, Y. (2013) *Escherichia coli* transcription termination factor NusA: heat-induced oligomerization and chaperone activity. Sci. Rep. 3, 2347.
[4] Yamashita, D., Sugawara, T., Takeshita, M., Kaneko, J., Kamio, Y., Tanaka, I., Tanaka, Y. and Yao, M. (2014) Molecular basis of transmembrane beta-barrel formation of staphylococcal pore-forming toxins. Nat. Commun. 5, 4897.
[5] Mechaly, A.E., Bellomio, A., Gil-Cartón, D., Morante, K., Valle, M., González-Mañas, J.M. and Guérin, D.M. (2011) Structural insights into the oligomerization and architecture of eukaryotic membrane pore-forming toxins. Structure 19, 181–191.

[6] De, S. and Olson, R. (2011) Crystal structure of the *Vibrio cholerae* cytolysin heptamer reveals common features among disparate pore-forming toxins. Proc. Natl. Acad. Sci. USA 108, 7385–7390.
[7] Song, L., Hobaugh, M.R., Shustak, C., Cheley, S., Bayley, H. and Gouaux, J.E. (1996) Structure of staphylococcal alpha-hemolysin, a heptameric transmembrane pore. Science 274, 1859–1866.
[8] Yamashita, K., Kawai, Y., Tanaka, Y., Hirano, N., Kaneko, J., Tomita, N., Ohta, M., Kamio, Y., Yao, M. and Tanaka, I. (2011) Crystal structure of the octameric pore of staphylococcal gamma-hemolysin reveals the beta-barrel pore formation mechanism by two components. Proc. Natl. Acad. Sci. USA 108, 17314–17319.
[9] Tanaka, K., Caaveiro, M.M.J., Morante, K., González-Mañas, J.M. and Tsumoto, K. (2015) Structural basis for the self-assembly of a cytolytic pore lined by protein and lipid. Nat. Commun. 6, 6337.
[10] Bellomio, A., Morante, K., Barlic, A., Gutiérrez-Aguirre, I., Viguera, A.R. and González-Mañas, J.M. (2009) Purification, cloning and characterization of fragaceatoxin C, a novel actinoporin from the sea anemone *Actinia fragacea*. Toxicon 54, 869–880.
[11] Michael, S.F. (1994) Mutagenesis by incorporation of a phosphorylated oligo during PCR amplification. Biotechniques 16, 410–412.
[12] Mayer, L.D., Hope, M.J. and Cullis, P.R. (1986) Vesicles of variable sizes produced by a rapid extrusion procedure. Biochim. Biophys. Acta 858, 161–168.
[13] Bartlett, G.R. (1959) Phosphorus assay in column chromatography. J. Biol. Chem. 234, 466–468.
[14] Ellens, H., Bentz, J. and Szoka, F.C. (1985) H^+- and Ca^{2+}-induced fusion and destabilization of liposomes. Biochemistry 24, 3099–3106.
[15] Davies, J.T. and Rideal, E.K. (1961) Interfacial Phenomena, Academic Press, New York.
[16] Caaveiro, J.M., Echabe, I., Gutiérrez-Aguirre, I., Nieva, J.L., Arrondo, J.L. and González-Mañas, J.M. (2001) Differential interaction of equinatoxin II with model membranes in response to lipid composition. Biophys. J. 80, 1343–1353.
[17] Greenfield, N.J. (2006) Using circular dichroism collected as a function of temperature to determine the thermodynamics of protein unfolding and binding interactions. Nat. Protoc. 1, 2527–2535.
[18] Alegre-Cebollada, J., Cunietti, M., Herrero-Galán, E., Gavilanes, J.G. and Martínez-del-Pozo, Á. (2008) Calorimetric scrutiny of lipid binding by sticholysin II toxin mutants. J. Mol. Biol. 382, 920–930.
[19] de los Rios, V., Mancheno, J.M., del Pozo, A.M., Alfonso, C., Rivas, G., Onaderra, M. and Gavilanes, J.G. (1999) Sticholysin II, a cytolysin from the sea anemone *Stichodactyla helianthus*, is a monomer-tetramer associating protein. FEBS Lett. 455, 27–30.
[20] Smaby, J.M., Kulkarni, V.S., Momsen, M. and Brown, R.E. (1996) The interfacial elastic packing interactions of galactosylceramides, sphingomyelins, and phosphatidylcholines. Biophys. J. 70, 868–877.
[21] Calvez, P., Bussieres, S., Demers, E. and Salesse, C. (2009) Parameters modulating the maximum insertion pressure of proteins and peptides in lipid monolayers. Biochimie 91, 718–733.
[22] Morante, K., Caaveiro, M.M.J., Tanaka, K., González-Mañas, J.M. and Tsumoto, K. (2015) A pore-forming toxin requires a specific residue for its activity in membranes with particular physicochemical properties. J. Biol. Chem. 290, 10850–10861.
[23] Marianayagam, N.J., Sunde, M. and Matthews, J.M. (2004) The power of two: protein dimerization in biology. Trends Biochem. Sci. 29, 618–625.
[24] Ali, M.H. and Imperiali, B. (2005) Protein oligomerization: how and why. Bioorg. Med. Chem. 13, 5013–5020.
[25] Walden, H., Bell, G.S., Russell, R.J., Siebers, B., Hensel, R. and Taylor, G.L. (2001) Tiny TIM: a small, tetrameric, hyperthermostable triosephosphate isomerase. J. Mol. Biol. 306, 745–757.
[26] Anderluh, G., Barlic, A., Potrich, C., Macek, P. and Menestrina, G. (2000) Lysine 77 is a key residue in aggregation of equinatoxin II, a pore-forming toxin from sea anemone Actinia eguina. J. Membr. Biol. 173, 47–55.
[27] García, K.C. and Teyton, L. (1998) T-cell receptor peptide-MHC interactions: biological lessons from structural studies. Curr. Opin. Biotechnol. 9, 338–343.
[28] Mueller, M., Grauschopf, U., Maier, T., Glockshuber, R. and Ban, N. (2009) The structure of a cytolytic alpha-helical toxin pore reveals its assembly mechanism. Nature 459, 726–730.
[29] Clackson, T. and Wells, J.A. (1995) A hot spot of binding energy in a hormone-receptor interface. Science 267, 383–386.
[30] Yamaji-Hasegawa, A., Makino, A., Baba, T., Senoh, Y., Kimura-Suda, H., Sato, S.B., Terada, N., Ohno, S., Kiyokawa, E., Umeda, M. and Kobayashi, T. (2003) Oligomerization and pore formation of a sphingomyelin-specific toxin, lysenin. J. Biol. Chem. 278, 22762–22770.
[31] Signarvic, R.S. and Degrado, W.F. (2009) Metal-binding dependent disruption of membranes by designed helices. J. Am. Chem. Soc. 131, 3377–3384.